As originally published in the SMTA Proceedings

Reducing Dust Deposition on Electronic Equipment by Optimizing Cooling Air Flow Patterns

Chen Xu **Jason Stafford***
Nokia Imperial College London
Murray Hill, NJ, USA London, United Kingdom
*Worked at Alcatel-Lucent/ Nokia (Ireland) when the work was performed

Abstract
Environmental dust accumulation on electronic equipment can impact the performance and reliability of the equipment in various ways. This includes mechanical effects (such as obstructions of cooling air, moving parts and optical interference), chemical effects (such as corrosion and metallic dendrite growth) and electrical effects (such as impedance reduction, short and open circuits). Minimization of dust deposition on electronic equipment is necessary and beneficial to product performance and long-term reliability. This work focuses on one aspect of reducing dust accumulation on electronic equipment, specifically by optimizing the cooling air flow.

1. Introduction

The ubiquitous presence of environmental dust (including both solid and liquid particles) makes it unavoidable for it to be deposited on the electronic equipment. Modern electronics are designed to tolerate certain degrees of dust deposition. For instance, telecom equipment deployed in North America needs to pass the qualification test outlined in Telcordia GR-1274 "Generic Requirements for Reliability Qualification Testing of Printed Wiring Assemblies (PWAs) Exposed to Airborne Hygroscopic Dust" [1]. However, when the accumulation of dust on the electronic equipmentbecomes high enough, it can impact the performance and reliability of electronic equipment. The high dust deposition on electronic equipment is especially an issue in the regions where the concentration of the environmental dust is high, and the indoor environment is inadequately controlled.

Dust can impact electronic reliability in mechanical, chemical and electrical ways:

- Mechanical effects include obstruction of cooling air-flow and deposition on components to reduce heat transfer, interference with moving parts, abrasion, optical interference, interconnect interference, or deformation of surfaces (e.g., magnetic media) and other similar effects.
- Chemical effects include corrosion of surfaces, dendrite growth due to electrochemical migration, and material property changes such as embrittlement or optical clouding of surfaces.
- Electrical effects include impedance changes and electronic circuit conductor bridging due to electrochemical migration. Deposition onto contacts can cause degradation and accelerated corrosion of the contact surface and intermittent as well as permanent connection issues.

Dust particles can be generally divided into two categories: coarse and fine particles.

- Coarse Particles, with particle size larger than 2.5 μm in diameter, typically contain 5 to 20 % water soluble components and are derived largely from natural materials and have mineralogical composition.
- Fine Particles, with particle size between 0.1 -2.5 μm in diameter, typically contain 25 to 50% water soluble components and are derived from combustion processes (power plants and vehicles). Common air filters are not effective for removing submicron particles (see Table 1 and discussion below). The ionic species in fine particles can form conducting (electrolyte) solutions at RH > 55 -60%, leading to electrical leakage, arcing, and corrosion of conductor lines.

Air filters are widely used to remove dust from air circulation systems in buildings, rooms and equipment cabinets and chassis. The effectiveness of air filters in removing dust from the air stream is characterized by Minimum Efficiency Reporting Value (MERV). The MERV rating system was developed in 1987 by the American Society of Heating, Refrigeration and Air Conditioner Engineers (ASHRAE) and has values between 1 to 16. The higher the MERV value is the more efficient the filter will be in removing airborne particles. Table 1 shows the relationship between MERV rating and the dust trapping effectiveness of the air filter [2].

Table1 MERV Rating and Dust Removing Effectiveness

	MERV	1	2	3	4	5	6	7	8	9	10	11	12	13	14	15	16
Average minimum	0.3μm - 1.0μm													<75%	75-85%	85-95%	>95%
composite	1.0μm - 3.0 μm									<50%	50-65%	65-80%	>80%	>90%	>90%	>90%	>95%
efficiency	3.0μm - 10.0μm	20%	20%	20%	20%	20-35%	35-50%	50-70%	>70%	>85%	>85%	>85%	>90%	>90%	>90%	>90%	>95%

The downside of using air filters is the restriction of the air flow by the air filters, characterized by the pressure drop across the air filter. The pressure drop generally increases with increasing dust removing effectiveness, i.e., MERV value. The increased pressure drops, or high restriction of air flow will greatly reduce the heating or cooling efficiency of the equipment and lead to higher operating cost of the heating or cooling units. In selecting air filters for specific applications, removing as much dust as possible on one side has to be balanced against allowing sufficient air flows for the cooling on the other side. In most data or telecom centers, ASHRAE recommends the use of air filters with MERV rating between 11 and 13 for air entering the data center [3]. A fully sealed site with MERV 11-13 air filters installed will see most of the large dust removed but still some PM2.5 dust (dust with particle size smaller than 2.5 □m) entering the site. Some dust can also be generated inside of the equipment center or enter the site without going through the air filter (via doors or cracks, gaps or holes in the building etc.). At the equipment level, air filters with MERV ratings between 5-8 are often used to filter cooling air entering the chassis due to the high air flow required for cooling modern electronics. As Table 1 shows, air filters with MERV ratings between 5-8 is only effective for removing large particulates and do not remove PM2.5 particles. The most practical and cost-effective way for removing PM2.5 is at the room level. Once PM2.5 particles enter the site, they will pass through the chassis-level air filter and potentially deposit on the electronic equipment. Due to the chemical composition, PM2.5 particles pose the highest threat to the product reliability and are also most difficult to be removed.

Dust deposition on a surface is characterized by the deposition velocity, which is defined as the deposition rate (the number of particles depositing per unit surface area per unit time, $m^{-2}s^{-1}$) divided by the dust concentration, and therefore has units of $m*s^{-1}$.The deposition velocity depends strongly on the particle size, air velocity and flow pattern, chemical and physical structure of the surface. The large particles deposit on to the surface mainly through gravitational settlement, while the deposition of small particles on a surface is dominated by molecular diffusion (Brownian) and turbulent or eddy diffusion. Figure 1 shows the relationship between dust deposition velocity and particle size from various published measurements and theoretic prediction (solid lines), as summarized in Zhang's Ph.D. thesis [4].

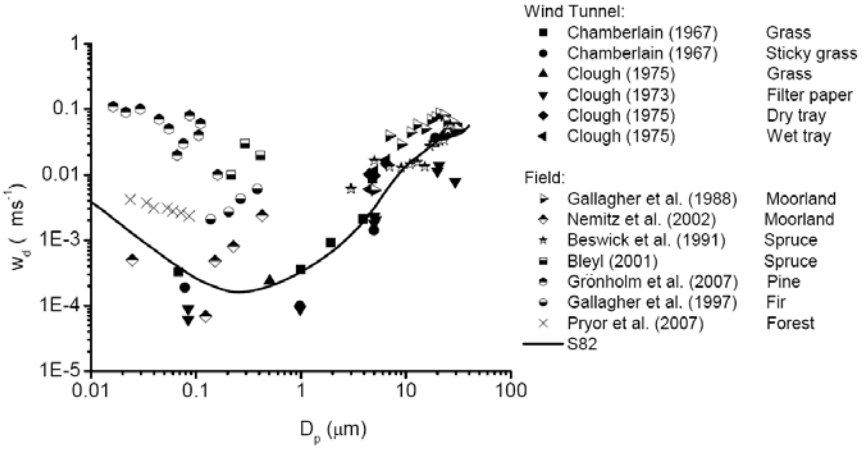

Fig. 1 Measurements of deposition velocities against particle size for different surfaces and a theoretic prediction [4].

For particles smaller than 0.1 microns, the particle deposition is dominated by the diffusion (Brownian and Eddy) and the deposition velocity decreases with increasing particle size. For particles larger than 0.5 microns, the particle deposition occurs primarily through gravitational settling and the deposition velocity increases with increasing particle size. As the result of these two competing deposition mechanisms, the particles between 0.1 and 0.5 microns have the lowest deposition velocity.

Dust deposition can also be accelerated by charges on dust particle (electrophoretic deposition), temperature gradient (thermophoretic deposition) and light (photophoretic deposition). However, their contributions are generally smaller than those from the diffusion and gravitational settling [5].

In the fan cooled equipment, the deposition velocity due to the diffusion (Brownian and Eddy)also depends strongly on the air velocity. For airflow parallel to the surface, the deposition velocity (v_d) on to the surface is directly proportional to the square root of the air velocity (u_a):

$$v_d = f\sqrt{u_a} \quad (1)$$

The proportional coefficient *f* depends on the type and size of the particles and is about 0.002 for 0.5um particle [6]. Tencer [6] has calculated deposition velocity due to the diffusion at two air velocities (0.5cm/s and 5cm/s) in dependence of particle sizes and compared this result with deposition velocity due to other mechanisms (gravitational settling, thermophoresis at 1K/cm and electrodeposition at 1.8V/cm). Tencer's result is reproduced in Figure 2.

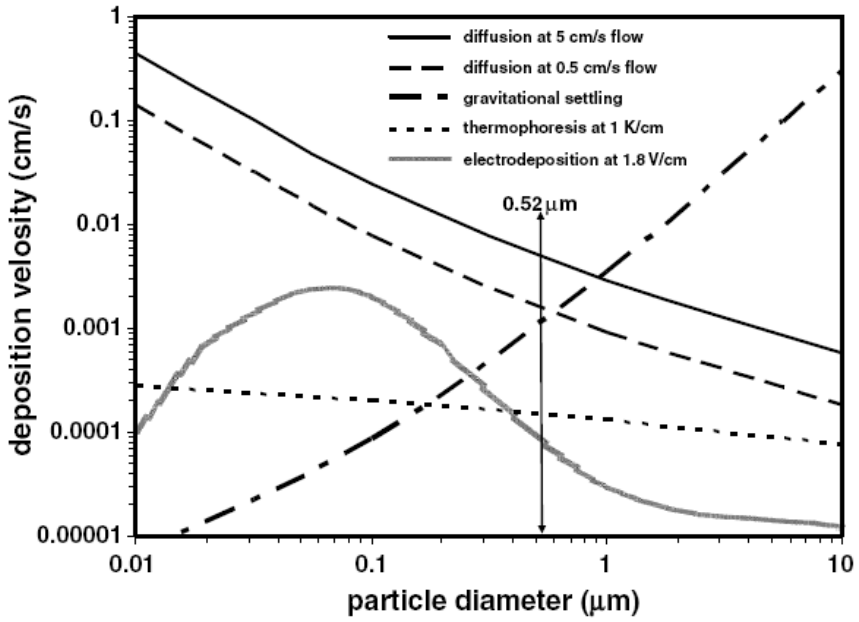

Figure 2. Dust deposition velocity on printed circuit boards due to different deposition mechanisms

As we can clearly see in figure 2, the dust deposition is dominated by diffusion for the particles smaller than 1 micron. For most fan-cooled equipment, the air velocity is typically 1 to5m/s, which will further increase the deposition velocity due to diffusion by a factor 5 or 10 compared to that at 5cm/s air flow according to equation (1). As discussed above, large particles will be effectively removed by the commonly used air filters and only micron and sub-micron sized particles (such as PM2.5) can reach the circuit boards in most cases. Also due to the chemical composition, micron and sub-micron sized particles pose the highest threat to the product reliability and their deposition on electronic products are mostly determined by the diffusion mechanisms.

In addition to linear air velocity, the deposition velocity depends also on the direction and flow pattern of the cooling air. In the extreme case of air flow direction being perpendicular to the surface of the circuit board (compared to being parallel to the surface), the deposition velocity equals to air velocity:

$v_d = u_a$(2)

For the two extreme cases of air flow direction in relationship to the surface of the circuit board (parallel and perpendicular), the deposition velocity can be different by a factor of ~500 between the two cases.

2. Experimental

Observations of various air-cooled equipment operating in the field highlighted a region of elevated levels of dust deposition, typically in the direct downstream of cooling fans. Acellular base station was chosen to study the general mechanisms behind this localized preferential dust deposition. For this equipment, deposition occurred on the mainboard (Figure 3a) and adjacent to the cooling air flow exiting the fan tray (Figure 3b). Interestingly, this localized preferential dust deposition was also observed on the top cover of the equipment in many cases. Figure 4 illustrates an example from different equipment.

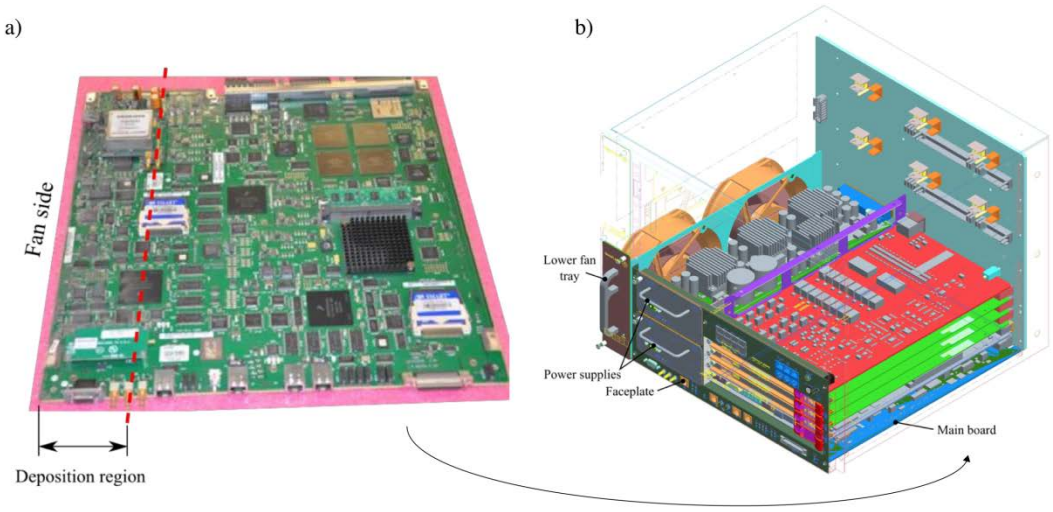

Figure3 – a) An image of the mainboard taken from the field and b) the location of this PCB within the cellular base station.

Figure 4. Preferential localized dust deposition on the top cover.

Particle image velocimetry (PIV) was implemented to study the local airflow behavior and the underlying mechanism behind the deposition process. A flow control strategy was designed based on this information, to reduce the mechanism driving the deposition of dust.

The experimental arrangement is shown in Figure 5. The equipment was rack-mounted along with an external power supply that was used to control the rotational speed of bothaxial fans. This arrangement was contained within a dedicated testing environment approximately 8 m (L)× 3 m (W)× 3 m (H). Minor modifications to the equipment faceplate were necessary to gain optical access for recording velocity field data near the deposition region. Three measurement planes outlined in Figure 6a) (green planes) were examined. Similar observations were noted for all three planes, therefore, a single centrally located plane has been chosen for the analyses (Figure 6 b). A laser sheet with 532 nm wavelength was generated using a production Nd-YAG Laser. The laser sheet illuminated glycol-based tracer particles (<10 μm in diameter) twice in succession for three different two-dimensional measurement planes shown in Figure 5. The tracer particles were introduced into the test environment using a production 2500Hz hazer and a production Haze Fluid (relative density of 1.05 at 20 °C). A homogeneous particle distribution was achieved after approximately 10 min of continuous issuing of tracer particles. Once sufficient tracer particle density was achieved, the hazer was turned off for 1 minute prior to recording velocity field data. A production 4MP CCD camera was positioned perpendicular to the laser sheet plane to record the scattered light from the particles on two separate frames for the regions of interest shown in Figure 6. The camera and laser were synchronized using a production laser pulse synchronizer. Each image pair was split into interrogation regions that were 32 × 32 pixels and processed using production 4G software. Timing between laser pulses was adjusted based on air velocities at each operating point considered. The timing was selected to ensure that the relative image displacement was kept below or equal to 0.25 for each interrogation region, as recommended by Keane and Adrian [7]. For the velocity data presented in this paper, the resultant timing set between pulses was in the range 8μs<□t < 100 μs. Velocity vector fields presented in this paper have a spatial resolution of 250μm and were acquired at a frequency of 7.5 Hz.

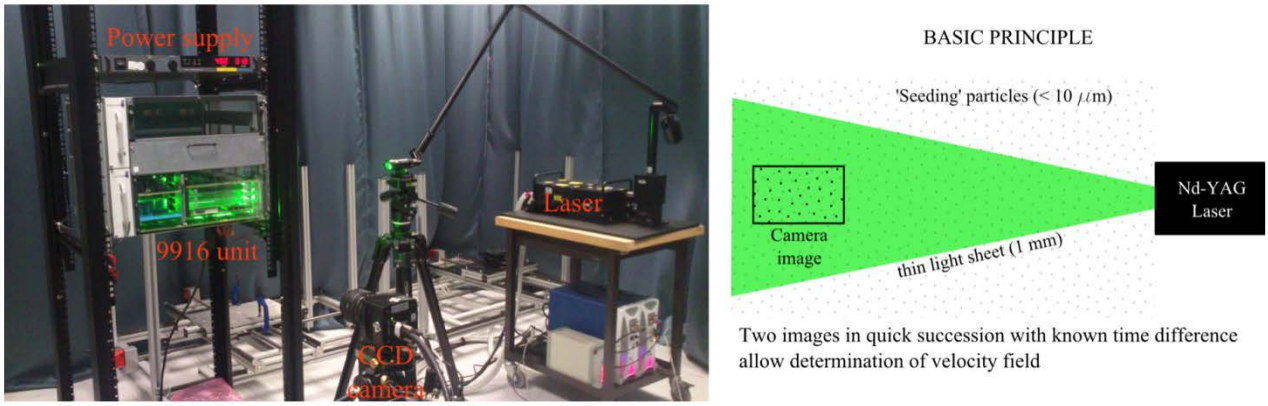

Figure 5 – Experimental setup for PIV

Fixed errors for the PIV system were estimated to produce a relative uncertainty in a velocity magnitude of <2%. A production air quality monitor was used to estimate the particle size that was generated from the hazer. This provided a measurement for particulate matter PM2.5 (diameters less than 2.5 μm) and PM10 (diameters between 2.5 and 10 μm). Over 90% of the particles sensed were in the range PM2.5. Using a conservative particle diameter of 5 μm in Stoke's law, the velocity slip error was calculated to be <1.8% for the glycol-based seeding [8, 9]. The particle image density (N_I) was 17 <N_I < 25 per interrogation region, ensuring that a high probability of valid detection rate was achieved (>95%) [7, 9]. This choice of particle image density also lowered the measurement uncertainty in particle image shift as recommended by Raffel *et al.* [10]. This assessment was based on an average particle concentration across all interrogation regions of the image, and any local differences in particle concentration were deemed negligible by maintaining uniform seeding density. A minimum of 1000 image pairs were recorded for each operating condition of interest. The convergence of full field measurement statistics was considered using the approach by Stafford *et al.*[11]. The ensemble average velocity field sufficiently converged toward the time average within 5% using this sample size.

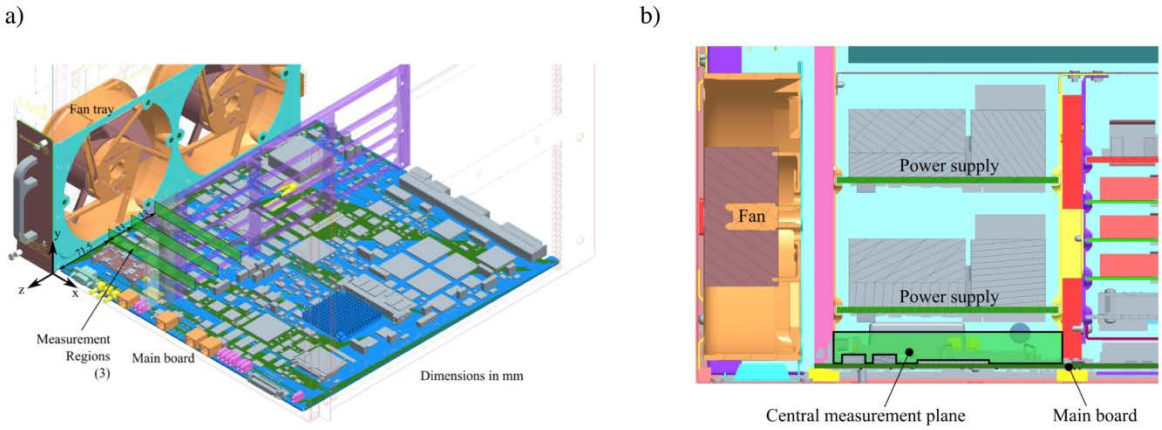

Figure 6 – a) An isometric view and b) a side view of the measurement planes for PIV

3. Results and Discussion

3.1 Velocity fields

Velocity fields for three locations in the central measurement plane (Figure 6) are shown in Figure 7. Both the ensemble-averaged (top row) and instantaneous (bottom row) velocity magnitude and streamlines demonstrate the varied flow that exists both spatially and temporally. There are, however, two distinct trends in the flow behaviour. In the first location (1) closest to the fan outlet, the fluid has the highest velocities and approaches the mainboard and components at an oblique angle. In contrast, the streamlines in locations 2 and 3 are almost parallel to the surface.This characteristic of an oblique impingement followed by flow that is almost parallel to the mainboard surface was found to be independent of rotational speed (for operating speeds 3000-5000 rpm). This is illustrated in Figure 8, which compares the velocity fields at two different rotational speeds. Although the magnitude increases, the angle of impingement is consistent as indicated by the similarity between streamlines.

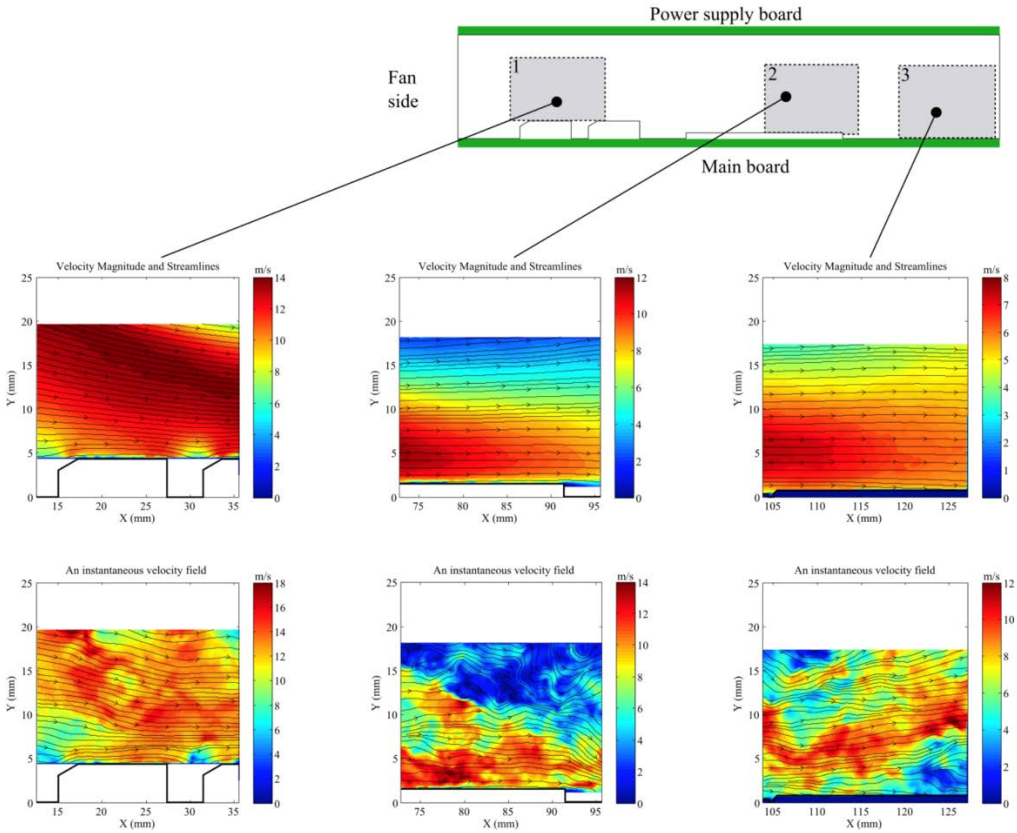

Figure 7 – Ensemble average and instantaneous velocity fields at three locations

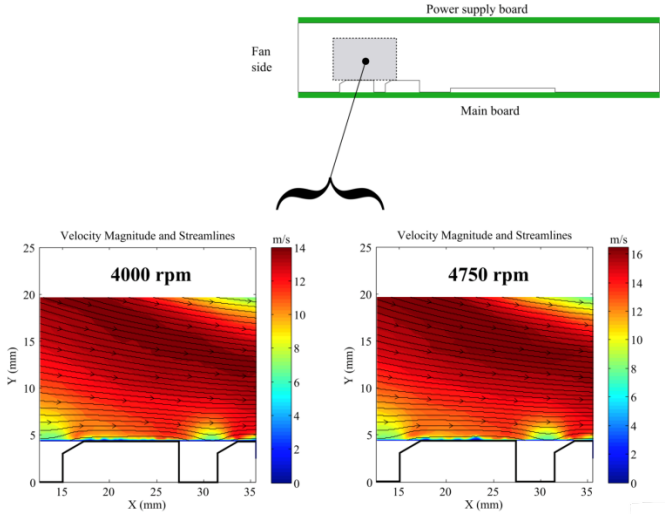

Figure 8 – Velocity fields for two different fan rotational speeds

Figure 9 shows the region where high dust deposition is located (zone A, see also Figure 1). This is distinguished from a downstream region (zone B) where the dust deposits were found to be negligible. The velocity measurements also indicate a notable change in the flow fields in each of these zones. Taking a point in the flow field approximately 5mm above the mainboard surface, the flow in the deposition region has an oblique angle of impingement which is an average -19 degrees from the horizontal. This average is surrounded by temporally varying data, however, it is clear from Figure 9 that most of the time the flow from the fan is pointed in an oblique direction towards the main board surface. In contrast, the downstream zone flows parallel (angle of 0 degrees) to the mainboard surface. Combined with lower absolute velocity magnitudes, the parallel flow characteristic in the downstream region reduces dust deposition. Velocity profiles are shown for 4 different locations on the mainboard in Figure 10, highlighting the significantly larger velocity gradients that occur within the deposition region. Momentum thickness is related to the diffusion boundary layer thickness [6], and high mass transfer rates occur in the regions where there is deposition on the mainboard. The deposition velocity in this region is more than two orders of magnitudes higher than outside the deposition region due to the combined effects of high exit flow velocity and

oblique flow impingement which is the primary deposition mechanism. This is illustrated in Figure 11. This deposition velocity estimate is based on using the scaling relationship in (1) in the downstream region, where the mean velocity was observed as parallel (see Figure 9). In the upstream region, impingement existed, and the normal component of velocity (V_i)was treated as an impingement velocity in (2).

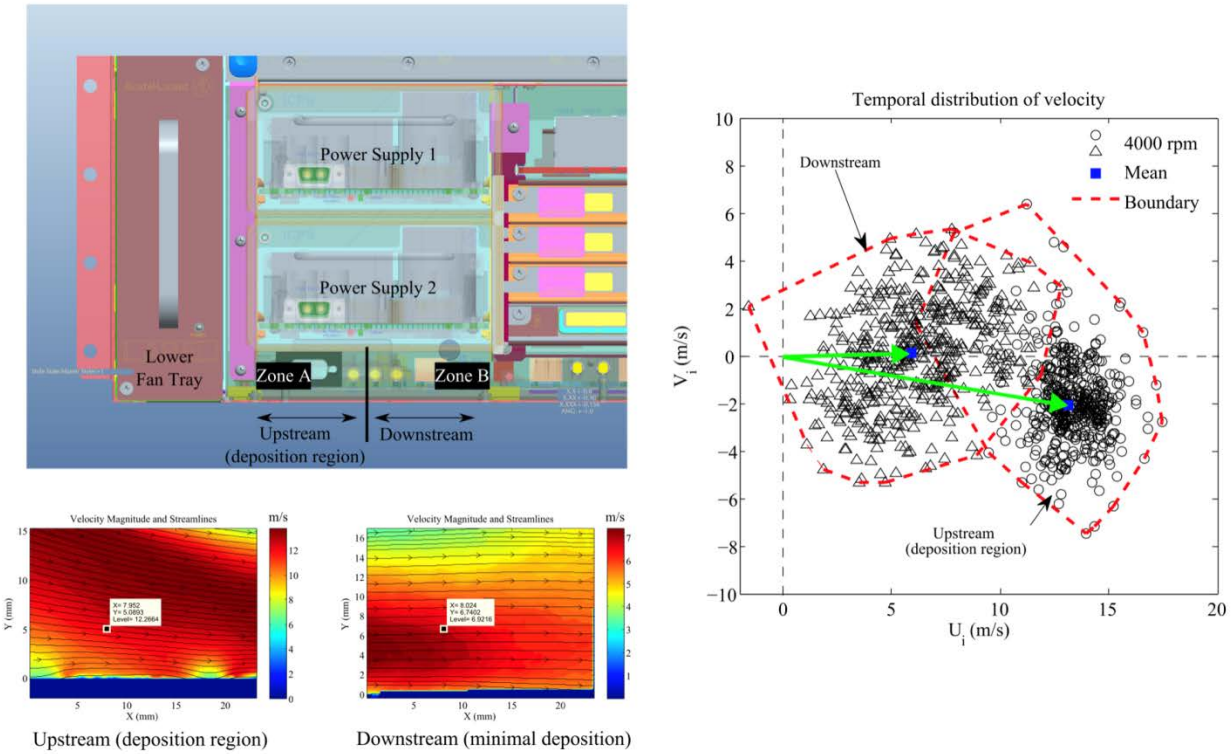

Figure 9 – Angle of airflow within and outside the dust deposition region. Two points in the upstream and downstream regions have been identified (bottom left). On the right, the change in velocity with time for both sample points (circle = upstream, triangle = downstream).

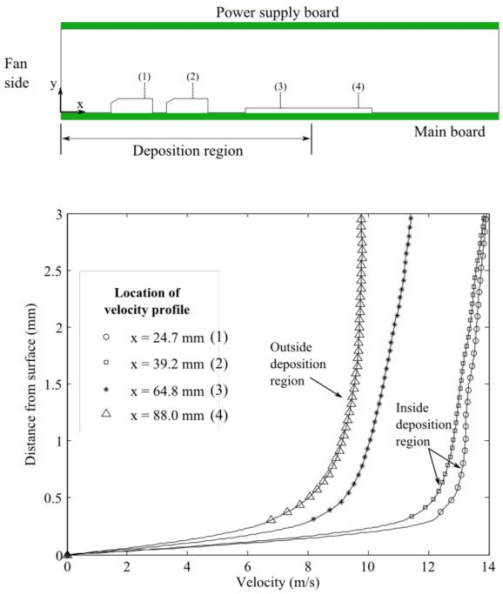

Figure 10 – Velocity profiles within and outside the deposition region

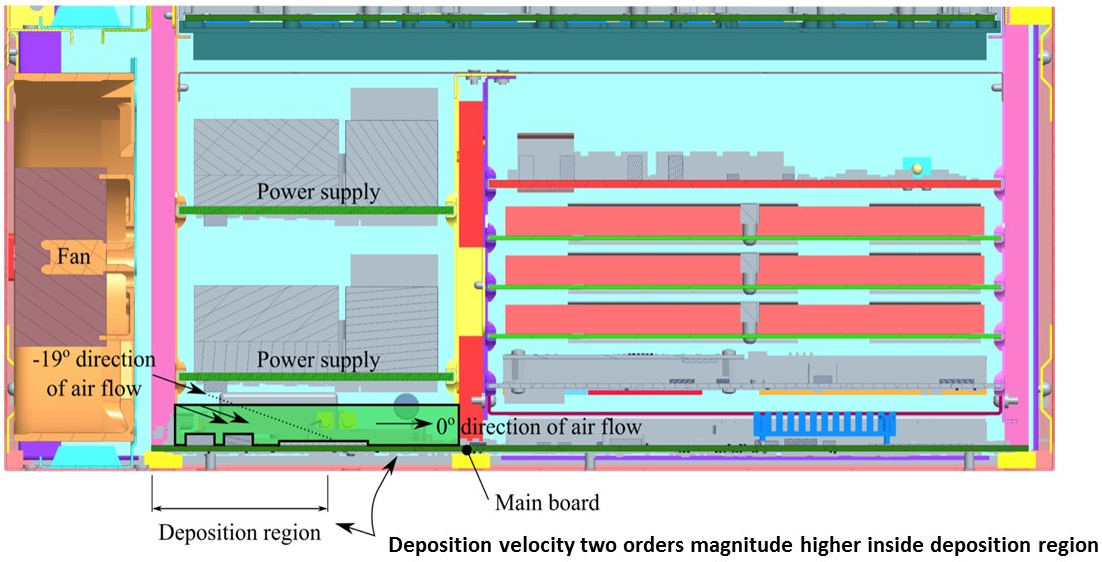

Figure 11 – Angle of impingement, deposition region and enhancement to deposition velocity

3.2 Adverse effects of traditional air filtering

The traditional approach to alleviating dust problems in electronic equipment is through filtering the cooling air that enters. To test the effect this may have on the dust deposition mechanism described above, tests were conducted using various filter grades listed in Figure 12. The filter was positioned at the inlet side of the axial fans, and particle image velocimetry was used to measure changes to the exit flow angle within the equipment. It is noted that this approach was possible given that 90% of the seeding particles were measured to be PM2.5 (see section 2), and predominantly passed through the filters allowing velocity measurements of the exit flow. The results shown in Figure 12 demonstrate the change in the oblique angle of impingement from approximately -19 degrees without filtering to -25.5 degrees using a high efficiency MERV7 filter. An experiment, illustrated in Figure 13 a), was conducted on the fan tray in isolation to analyse this further. It involved placing threads, or tufts along the fan hub supports which aligned with the flow in the fan exit plane. Then, different filters were placed on the inlet side and the flow angle was subsequently measured. Examples of these images are shown in Figure 13 b). The filters have a substantial effect on the exit flow, changing the operating point of the fan (Figure 14). At a constant rotational speed, filters reduce the axial flow component and the centrifugal forces within the fan exit flow. This, in turn, changes the exit flow angle, as illustrated in Figure 14.When considering that the primary mechanism behind deposition is the oblique flow impingement, these results highlight that adding filters could adversely increase the dust deposition problem. This is particularly important if the particle content is predominantly PM2.5 and the filters are designed for only removing large particles (> 3 □m).

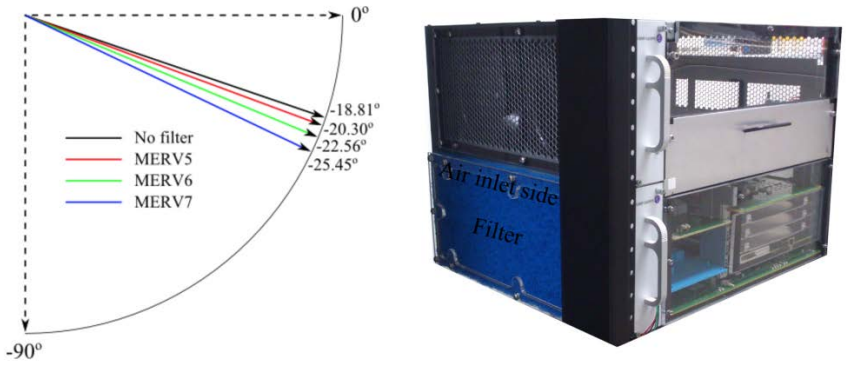

Figure 12 – Changes to the fan exit flow with the addition of traditional filtering

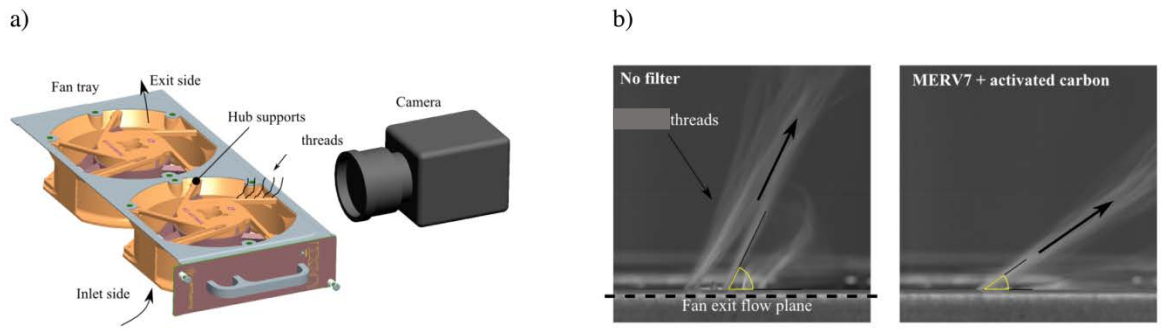

Figure 13 – a) Isolated experiment to measure the effect of inlet side filtering and b) the resultant images showing the effect of filters on fan exit flow angle

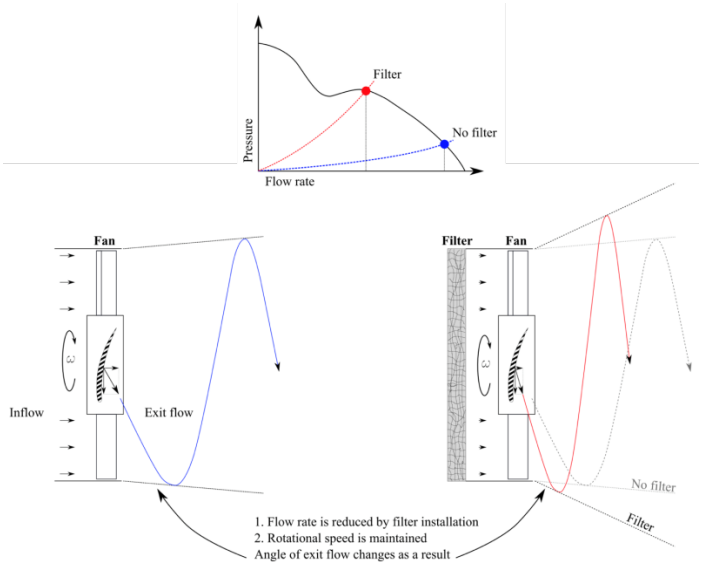

Figure 14 – Illustration of filter-induced alteration to fan operation and local exit flow

3.3 Flow control as an alternative solution

An alternative approach to reducing dust deposition in electronic equipment is to control the flow exiting the fan. The concept is to locally alter the exiting air flow angle so that the oblique flow impingement is lessened, while minimising adverse effects to the bulk aerodynamic performance of the fan (Pressure-Flow rate). This has been achieved on this equipment by integrating guide vanes at the fan exit, shown in Figure 15. A number of guide vane geometries were tested to find a suitable solution that aligned the flow with the mainboard. A sample of these are shown in Figure 16. The guide vanes which performed the best, were designed to have a flow entrance angle equal to the measured fan exit flow angle (i.e. -19 degrees). The vane exit angle was designed such that the air flow leaving the vane was parallel to the mainboard. A numerical simulation of the fan tray and aerodynamic guide vanes (Figure 17) was implemented to investigate the loss to global fan performance. Up to a 5% reduction in volumetric flow rate was predicted using production simulation software and a zero-equation turbulence model. The flow introduced into the computational domain due to the fan rotation was modelled by implementing a characteristic pressure-flow rate curve that matched the fans used in the equipment. The domain dimensions matched the equipment dimensions. No-slip boundary conditions were provided to the vanes and walls of the domain. The exit of the domain was modelled as a pressure outlet. This minimal reduction in flow rate is particularly favourable when considering that losses due to high efficiency filters can be greater than 50%. The benefits of these vanes, therefore, are that they can be retrofitted (shown here)and also have a negligible impact on bulk aerodynamic performance. This is important for maintaining the thermal performance of the equipment while also addressing the reliability challenges of dust deposition.

Figure 15 – Integrated guide vanes for local flow control at the fan exit

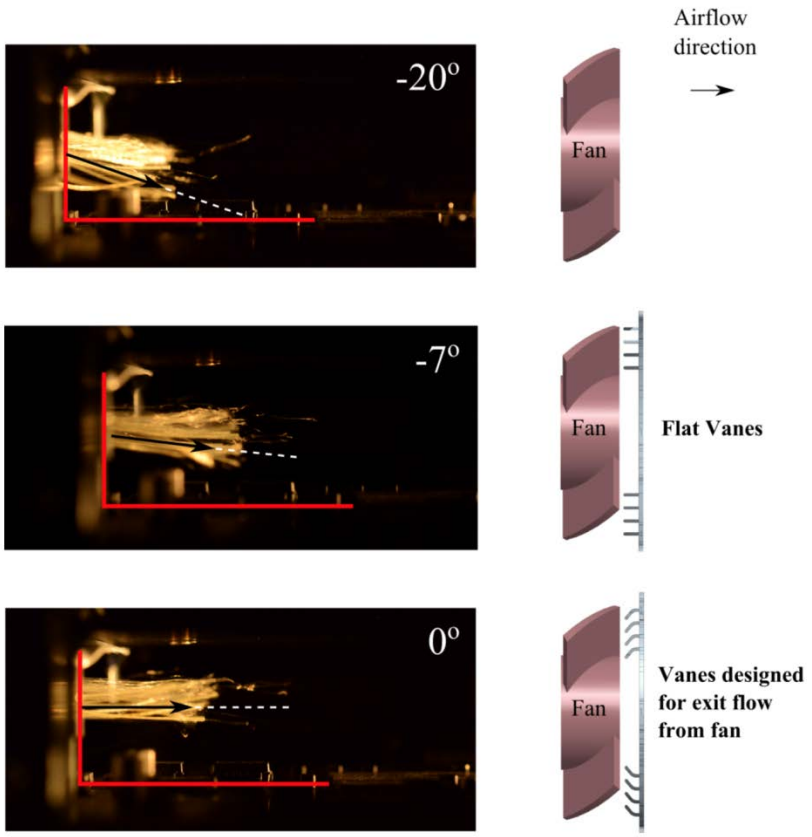

Figure 16 – Tuft measurements (left) for different guide vane geometries (right)

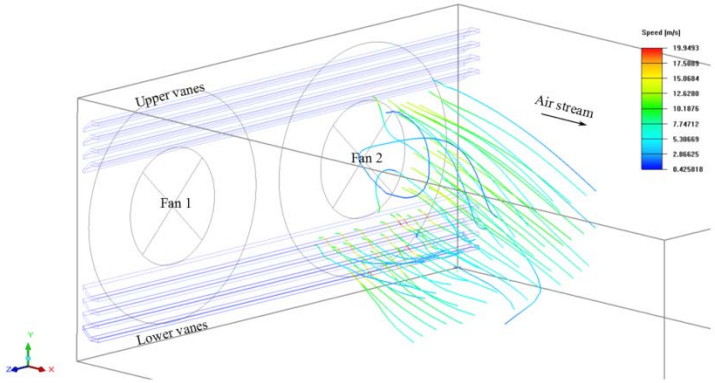

Figure 17 – Numerically predicted streamlines through the selected guide vane geometry

4. Conclusions

This work presents a detailed analysis on dust deposition mechanisms in air cooled electronic equipment using particle image velocimetry performed *in situ* on a cellular base station. Localized preferential dust deposition is driven by high velocity air flowing at an oblique angle at the exit of rotating axial fans. This oblique angle is a characteristic of all rotating axial fans, due to centrifugal forces in the exiting jet. This produces locally increased deposition velocities that is more than two orders of magnitude higher in zones where dust deposition was observed in the field. It was demonstrated that the addition of traditional filters on the fan inlet side may worsen the situation by enhancing the deposition mechanism through changes to the impingement angle. Finally, a method is proposed which uses aerodynamic guide vanes to control the flow locally, reducing the deposition mechanism while having negligible effect on the bulk fan performance. This work also highlighted the importance of maintaining low concentration of PM2.5 dust (most detrimental dust to electronic equipment) at the data center and the most practical and cost-effective way for removing PM2.5 is at the room level.

5. References

[1] GR-1274-CORE, "Generic Requirements for Reliability Qualification Testing of Printed Wiring Assemblies (PWAs) Exposed to Airborne Hygroscopic Dust", Issue 2, November 2009

[2] ANSI/ASHRAE Standard 52.2-2012, "Method of Testing General Ventilation Air-Cleaning Devices for Removal Efficiency by Particle Size"

[3] ASHRAE Datacom Series, "Particulate and Gaseous Contamination in Datacom Environments", Second Edition 2014

[4] J. Zhang, "A Study on Dust Dry Deposition: Wind-tunnel Experiment and Improved Parameterization" Ph.D. thesis, 2013

[5] C. I. Davidson and Y.L. Wu, "Dry deposition of particles and vapors. Acidic precipitation" 1990 (pp. 103-216). Springer, New York.

[6] M. Tencer, "Deposition of aerosol ("hygroscopic dust") on electronics – Mechanism and risk," *Microelec. Rel.*, vol. 48, no. 4, pp. 584–593, 2008.

[7] R. D. Keane and R. J. Adrian, "Optimization of particle image velocimeters. I. Double pulsed systems," *Meas. Sci. Technol.*, vol. 1, no. 11, pp. 1202–1215, 1990.

[8] L. Lading, G. Wigley, and P. Buchhave, *Optical Diagnostics for Flow Processes*. New York, NY, USA: Springer, 1994.

[9] J. Stafford and N. Jeffers, "Aerodynamic performance of a vibrating piezoelectric blade under varied operational and confinement states," *IEEE Trans. Comp. Pack. Manu. Tech.*, vol. 7, no. 5, pp. 751–761, 2017.

[10]M.Raffel, C. E. Willert, S. T. Wereley, and J. Kompenhans, *Particle Image Velocimetry: A Practical Guide*, 2nd ed. Berlin, Germany: Springer-Verlag, 2007.

[11] J. Stafford, E. Walsh, and V. Egan, "A statistical analysis for time-averaged turbulent and fluctuating flow fields using particle image velocimetry," *Flow Meas. Instrum.*, vol. 26, pp. 1–9, 2012.